Rift-parallel block-like motion of the graben floor during the 2005-2010 Afar rifting episode

Yuji Himematsu[1, 3], Masato Furuya[2]

1. Department of Natural History Sciences, Graduate School of Science, Hokkaido University Sapporo, Japan
2. Department of Earth and Planetary Sciences, Faculty of Science, Hokkaido University, Sapporo, Japan
3. Now at Volcano Disaster Resilience Research Division, National Research Institute for Earth Science and Disaster Resilience, Tsukuba, Japan

Corresponding author: Yuji Himematsu

E-mail: himematsu@bosai.go.jp

Postal address: 3-1 Tennodai, Tsukuba 305-0006, Japan

Voice: +81-29-863-7303

Keywords: Afar, Satellite SAR, Pixel tracking, Rifting episode, the East African Rift, ALOS/PALSAR

Abstract

Crustal deformations associated with rifting episodes are often explained by both normal faulting and tensile opening in an elastic body, suggesting no significant rift-parallel displacements. In this study, using ALOS/PALSAR pixel-offset and multiple aperture interferometry (MAI) data, we detected ~1 m of northwestward block-like cumulative horizontal motion in the graben floor during the latter half of the 2005-2010 Afar rifting episode, Ethiopia. This horizontal block-like motion can be explained by additional shallower strike-slip on normal fault surfaces, which was presumably aseismic due to the very small number of strike-slip earthquakes and a significant gap between seismic and geodetic moment releases. We conclude that the rift-parallel movement can be interpreted by the strain accommodation of plate oblique spreading associated with dike intrusions, as has been demonstrated for the 2014 Bárðarbunga dike intrusion episode. Although we do not propose direct evidence for the plate oblique spreading, the complicated tectonic setting caused by the rotation of the Danakil block and the upwelling plume beneath the Afar triple junction may be drivers of the rift-parallel motion associated with the Afar dike intrusion.

1. Introduction

The Afar depression is located at a triple junction of the subaerial divergent plate boundaries between the Arabian, Somalian, and Nubian plates at the northernmost part of the East African Rift (EAR; Fig. 1) (e.g., McKenzie et al., 1970; Saria et al., 2014). While geodetic observations indicate the steady spreading along the East African Rift (Kreemer et al., 2003; Stamps et al., 2008), dike intrusion episodes intermittently occur along the continental rift zones, accompanying significant ground displacement (Calais et al., 2008; Wright et al., 2006). The 2005-2010 Afar rifting episode was a long-lasting dike intrusion episode that occurred along the Manda

Hararo-Dabbahu magmatic segment, which is located on the boundary between the Nubian and Arabian plates (Fig. 1). The episode consisted of 14 discrete dike intrusions, the first of which induced the largest amount of magma intrusion (~2.5 km^3) (e.g., Wright et al., 2012). Previous geodetic studies have inferred three-dimensional (3D) displacements that were caused by the September 2005 event based on satellite synthetic aperture radar (SAR) and optical images (e.g., Wright et al., 2006; Grandin et al., 2009, 2010; Hamling et al., 2009). The spatial pattern of the derived crustal deformation showed an archetypical graben structure, with the uplifted graben shoulders extending from NE to SW and the narrow graben floor subsided by up to 3 m (Wright et al., 2006; Grandin et al., 2009, 2010b; Hamling et al., 2009).The dike opening model for the 2005 mega dike intrusion suggested that the magma was fed from at least three sources; two sources located beneath Gabho and Dabbahu volcano and another source located beneath the center of the Manda Hararo magmatic segment (Ado' Ale volcanic complex). Additionally, the ground displacements of subsequent events after June 2006 (Events 2-14) have been derived from interferometric SAR (InSAR) data. However, displacement data over the graben floor were lacking because of the phase decorrelation problem of the C-band ENVISAT data (Hamling et al., 2009; Hamling et al., 2014); we follow Hamling et al. (2009) and Wright et al. (2012) for the numbering of the sequential events, with the September 2005 event being denoted as Event 1. Their observations implied that the magma was mainly supplied from Ado' Ale volcanic complex but their depths vary for the subsequence dike intrusion episode. Although some previous studies have presented 3D displacement fields that were associated with the rifting events since 2006 (Grandin et al., 2010a; Hamling et al., 2014; Pagli et al., 2014), these fields were derived by interpolating the displacement data outside the graben floor into the data-missing graben floor. Therefore, it remains uncertain whether the graben was simply subsiding without any horizontal displacements.

Himematsu and Furuya (2015) reported significant rift-parallel block-like horizontal motion at the subsiding graben floor in the 2007 Natron rifting event by analyzing Phased-Array type L-band Synthetic Aperture Radar (PALSAR) images that were obtained by the Advanced Land Observation Satellite (ALOS). These displacements were explained by strike-slips on the two graben-bounding faults, which, to our knowledge, has never been reported in any previous rifting events. Very few strike components in seismological data and a gap of seismic and geodetic moment release suggest that these strike-slips were aseismic. According to the USGS catalog, the focal mechanisms during the 2005-2010 Afar dike intrusion episode were mostly dominated by normal faulting with few strike-slip components (Fig. 1). However, no similar rift-parallel horizontal displacements were reported in the 2005-2010 Afar rifting event, and the frequency and universality of the rift-parallel movements remain uncertain. Similar horizontal displacement on a graben floor was reported by Ruch et al. (2016) in the Bárðarbunga dike intrusion episode in 2014 in Iceland; see also Himematsu et al. (2019). They proposed that the symmetric horizontal displacements toward a minor fissure on the graben floor can be explained by the accommodation of shear strain caused by oblique plate spreading. Here, we reexamine crustal deformation data that were acquired from PALSAR data in order to determine if such rift-parallel movements accompanied the 2005-2010 Afar rifting events; the details of the PALSAR images are shown in Table S1 in the Supplementary Material. Moreover, no observation results for the Afar dike-intrusion episode based on PALSAR images have yet been reported. The advantage of L-band PALSAR data over shorter-wavelength data is their higher coherence even for long temporal separations, which allows us to monitor long-lasting displacements. To reduce the phase decorrelation problem, we apply an intensity-based pixel-offset technique (Strozzi et al., 2002), which should provide us with robust data rather than InSAR.

2. PALSAR Data Processing and Observation Results

A pixel-offset technique can provide us with two independent displacement datasets that are sensitive to both the line-of-sight direction (range offset) and the along-track direction (azimuth offset) (Tobita et al., 2001; Jónsson et al., 2002; Simons et al., 2002; Kobayashi et al., 2009). Processed images were acquired only from the ascending track, and thus did not allow us to completely resolve the 3D displacements. However, it was possible to constrain the displacement field using the range and azimuth offset data in the present satellite track, as the satellite flight direction is nearly parallel to the rift axis, and the range and azimuth offsets are sensitive to displacements that are perpendicular and parallel to the rift axis, respectively. The high coherence over a longer temporal separation in the L-band SAR data is even more important and helpful to robustly constrain the displacements. ALOS/PALSAR was launched in January 2006 and the images became available since 2007 in this study area, so we cannot quantify the surface displacements from earlier events in 2005-2006.

For the PALSAR data processing, we used the commercial GAMMA software (Wegmüller and Werner, 1997). When performing the pixel-offset technique, the search window size was set to 64×192 pixels (~600×620 m) for the range and azimuth directions with a sampling interval of 16×36 pixels (~150×120 m). Stereoscopic artifact was reduced by using the 3-arcsec (90 m) Shuttle Radar Topography Mission (SRTM) digital elevation model (DEM)) (Farr et al., 2007; Kobayashi et al., 2009).While both the range and azimuth offset indicated that the displacements were distributed over the ~40 km-long graben structure (Fig. 2), the azimuth offset showed a positive signal (towards N349°E) greater than 1 m over the northern half of the graben floor, and no such positive signals can be observed outside the graben floor (Fig. 2b). Time series of the

pixel-offset results are shown in Fig. S1 in the Supplementary Material, and the details of the dataset are given in Table S2 in the Supplementary Material. Additionally, the offset fields between the graben floor and the shoulders were clearly discontinuities. In particular, the graben floor moved along the satellite flight direction independently from both sides of the graben. These positive signals in the azimuth offset imply that rift-parallel horizontal movements did indeed occur, as was observed during the 2007 Natron event. Multiple aperture interferometry (MAI) (Bechor and Zebker, 2006), which is a phase-based method to detect horizontal displacements along satellite tracks, also indicated the same signals as the azimuth offset data (Fig. 2c). Thus, the rift-parallel horizontal displacements at the graben floor have been occurring since at least 12 June 2007. Given the presence of discontinuities in both the range and azimuth offsets across the boundaries between the graben floor and both sides of the graben, we can easily rule out that the rift-parallel motion was directly driven by volume changes in a shallow magmatic source. However, the presence of such a source at much deeper depths cannot be ruled out. We will further discuss the mechanisms of this movement in the following sections.

Casu and Manconi (2016) showed short-baseline time series of pixel-offset data by using a C-band ENVISAT/ASAR dataset during the post-2005 rifting event. Although they did not insist on rift-parallel motion in the graben floor, we clearly identified ~80 cm of northward rift-parallel movements in the displacement velocity from 2006 to 2010 (see Fig. 6b in Casu and Manconi, 2016). Namely, the rift-parallel motion in the graben floor during the post-2005 rifting event was confirmed based on both L-band and C-band data. Meanwhile, in view of the 3D displacement for the largest event in September 2005 as shown by Wright et al. (2006) and Grandin et al. (2009), few rift-parallel displacements could be observed.

In this study, to examine whether any relationship existed between the rift-parallel movements and the intruded magma volume, we compared the temporal evolution of the azimuth offset data with the estimated volume of magma injection during each rifting event by Hamling et al. (2010) and Wright et al. (2012) (Fig. 3). In the azimuth offset on the northern half of the graben floor, the azimuth offset started to increase in the northern part of the graben floor at the end of 2008 (Fig. 3a). The temporal characteristics of the azimuth offset correlated with the evolution of the range offset (graben formation) in the northern part of the graben floor. Most of the dike identified during 2007-2008 intruded to the southward (Fig. 3a), and thus we could identify few range and azimuth offsets in the northern half of the graben floor.

3. Fault source model

A fault slip distribution model in an elastic half space was constructed which could explain the cumulative displacements from June 2007 to August 2010 (Fig. 4 and Fig. S2 in the Supplementary Material). We applied quad-tree method to reduce the amount of data(Jónsson et al., 2002). The slip and tensile opening distribution model consisted of two graben-bounding faults and a pure vertical dike segment (Figs.4a-4f), which were constructed by triangular dislocation elements (Meade, 2007; Furuya and Yasuda, 2011). A Poisson's ratio of 0.25 and a rigidity of 30 GPa were assumed. When deriving the slip and tensile opening on each segment, we constrained both the slip direction and the smoothness of the inferred slip and opening distributions (Furuya and Yasuda, 2011; Himematsu and Furuya, 2015). The standard deviations of each component were derived by using 200-times iterative inversions with random noise (Wright et al., 2003) (Fig. S3 in the Supplementary Material). The slip distributions revealed that the strike slip was mostly concentrated near the surface, whereas the peak of the strike-slip (1.1 m at maximum) was located

158 at a depth of 2 km on the west-dipping fault. The cumulative geodetic moment release of the strike
159 components was 1.65×10^{18} Nm (Mw 6.08), while the total geodetic moment release, which
160 included both normal faulting and tensile opening, was 1.59×10^{19} Nm. The strike-slip
161 contributions in the geodetic moment release alone were five times greater than the cumulative
162 total seismic moment release (3.3×10^{17} Nm) during the observation period (Belachew et al., 2013).
163 Very few strike-slip earthquakes were detected by local seismic networks, and thus the gap in these
164 moment releases suggests that these strike slips were aseismic. The root-mean-square (RMS)
165 misfits were 12.9 cm and 7.0 cm for the range and azimuth offset, respectively.
166
167 Some previous models that were derived from ENVISAT/ASAR InSAR data proposed
168 approximately 3.5 m of cumulative dike opening since the 8th dike intrusion (Grandin et al., 2010b;
169 Hamling et al., 2010). In contrast, tensile opening was estimated to be 2.3 m in our best-fit model
170 even for the cumulative displacements, much smaller than previous estimates. However, neither
171 Grandin et al. (2010a) nor Hamling et al. (2010) included any fault segments in their models, only
172 using tensile openings, since the missing data in the graben floor meant that they did not have to
173 account for the consideration. On the other hand, other models by Ebinger et al. (2010) and
174 Hamling et al. (2009) included both tensile opening and fault segments, and provided the
175 cumulative opening from 2005 to 2009 (Ebinger et al., 2010; Hamling et al., 2009). The
176 accumulation diagram by Ebinger et al. (2010) indicated ~2.5 m of cumulative opening along the
177 southern part of the Manda Hararo-Dabbahu magmatic segment during 2007-2009, which is nearly
178 consistent with our estimated opening distribution. We consider that such models that include only
179 dike segments will overestimate the opening volume, and that the observed significant

displacements are likely related to tensile opening despite the presence of displacements from fault segments.

In the present study, we computed the Coulomb stress changes (ΔCFF) that were caused by tensile opening upon the two graben-bounding faults to assess if the dike intrusion promoted the inferred fault slip (Fig. 5) (King et al., 1994). Positive stress changes that correspond to unclamping were found to be concentrated at shallower depths (0-1.5 km) on each receiver fault. The distributions of positive stress changes were consistent with the inferred strike-slip distributions, however, the peak strike-slip was located at a depth of 2 km, where small negative stress changes were indicated. Thus, the stress changes caused by dike opening did not prevent aseismic strike-slip in the shallower part, and the stress changes are unlikely to have driven the rift-parallel motion.

4. Discussion

4.1 Aseismic slip consistent with the rate-and-state friction law

Our pixel-offset data and the fault model indicated that the observed displacements were mostly caused by aseismic processes since the cumulative seismic moment release can only explain less than 2% of the geodetic moment release. Aseismic slip plays a role in strain accommodation during rifting events (Calais et al., 2008) and can be one of the key drivers of earthquake swarms in volcanic or geothermal areas and divergent plate boundaries (Vidale and Shearer, 2006; Lohman and McGuire, 2007; Takada and Furuya, 2010; Wicks et al., 2011). According to the rate-and-state dependent friction law, aseismic slip tends to occur at shallower depths of the crust, where stable slip tends to occur (Dieterich, 1979; Ruina, 1983; Scholz and

Contreras, 1998). This slip tendency is consistent with our estimates of slip distribution, which indicate that strike-slip patches mostly occur at shallower depths than the normal faulting patches (Fig. 4).

4.2 Implication of the rift-parallel motion of the graben floor

The elastic fault model successfully explained the rift-parallel block-like motion on the graben floor associated with the dike intrusion episode, however, it did not clearly elucidate the dynamical mechanisms. One possible mechanism is strain accommodation of oblique plate spreading driven by dike intrusions (Ruch et al., 2016). In the 2014 Bárðarbunga dike intrusion episode, the rift axis was orientated at N25E, while the plate spreading around Bárðarbunga volcano is for the N104E, which is not completely perpendicular to the rift axis. Although most of the graben was located under an icecap (Himematsu et al., 2019), their observation results of Ruch et al. (2016) exhibited symmetrical horizontal displacements in the direction of the rift axis toward the area of maximum subsidence on the ice-free graben floor, indicating southward movements on the northern part of the ice-free graben floor and northward movements on the southern part of this region. For the temporal evolution of the displacement on the graben floor in Bárðarbunga, the increase of the SAR azimuth offset on the graben floor ceased in association with the decrease of seismic activity and the termination of graben evolution. Unlike the case of Bárðarbunga episode, the rift-parallel displacement in the Afar episode increased independently of the timing and volume of the dike intrusions (Fig. 3). The strain accommodation of oblique plate spreading may also have induced strike-slip earthquakes along the dike path in the Bárðarbunga episode

(Ágústsdóttir et al., 2016), while the focal mechanisms during the Afar episode reported the dominance of normal faulting component (Fig. 1).

In contrast, the chronology of the Afar depression based on geological data and numerical simulation suggests that the Afar depression was formed by the splitting with an anti-clockwise rotation of the Danakil block, that is, the boundary between the Nubian and Arabian plates is splitting nonuniformly (Collet et al., 2000; Corti, 2009). The motion of the Danakil block is driven by a rotation of the Arabian plate with a hinge fixed at the northernmost part of the divergent boundary between the Nubian and Arabian plate. The hinge locates at ~100 km southwestward away from a triple junction of seismicity at the middle part of the Red Sea, that is, about 100 km away from the coast of Eritrea for the NE direction (Fig. 1b). Several left-lateral earthquakes observed around the hinge of the Danakil block rotation imply the northward movement of the Danakil block with the anti-clockwise rotation (McClusky et al., 2010). Although there have been few observations which allow the identification of the spatial characteristics of long-term deformation around the Manda Hararo-Dabbahu rift segment, the rotation of the Danakil block or the Arabian plate would generate complex plate motion. Although there are several differences in the characteristics of the displacements in the graben floor between the Afar and Bárðarbunga dike intrusion episodes as described above, the strain accommodation of oblique plate spreading is a plausible explanation for our observation results.

The other possible mechanism is driven by the passive advection in the upper crust coupled with horizontally underlying flow of sill; this sill would have been deeper than 5 km because of the depth of the tensile opening (Fig. 4). In a recent thermo-rheological geodynamic model that aimed to reproduce the presence of both active and passive rift zones around the Tanzanian craton in the central EAR (Koptev et al., 2015), similar rift-parallel displacements were demonstrated

during dynamic topographic evolution. Significant gaps existed in terms of both the spatial and temporal resolutions between the thermo-rheological geodynamics model and our geodetic observations, and this model cannot yet reproduce episodic processes such as rifting, although these simulated rift-parallel displacements could be what we observed geodetically. A key simulated process that is relevant to the geodetic observations could be a channelized flow of plume material, which is the deflection of a plume head at the cratonic keel (Sleep, 1997; Albers and Christensen, 2001). A laterally channelized plume flow can generate narrow strain localizations and induce slow surface movements along rift axes (Koptev et al., 2015). Around Lake Natron in the simulation results, the surface velocity indicated southward horizontal movements on the order of a few millimeters per year, which is consistent with the direction of the rift-parallel displacements in the 2007 Natron rifting episode (Himematsu and Furuya, 2015).

The seismic tomography results showed low velocity zones at the southern edge of Afar, where we may expect an upwelling mantle plume (Bastow et al., 2008). The Moho depth distribution along the western-edge of Afar also indicates that the crustal thickness decreases towards the NNW (Hammond et al., 2011). If plume material flows along the rift axis in western Afar, this plume material would form a channel towards the NNW. This direction is also consistent with the rift-parallel movements over the graben floor in Afar. Assuming that this plume channeling causes along-axis surface velocity on the order of a few millimeters per year, as was suggested in the numerical model over the central EAR, the amplitude of the rift-parallel displacements (~1 m) in Afar is largely consistent with the strain that accumulates during one rifting cycle (~400 years) (Ebinger et al., 2010; Grandin et al., 2010a) and the surface velocity. However, the channelized plume flow may be an incompatible driver since it occurs at a deeper

depth, even though the numerical simulation can explain the rift-parallel movement as discussed above.

Even divergent plate boundaries under an extensional stress regime have the potential to generate strike-slip earthquakes. Accepted mechanisms for the generation of strike-slip earthquakes under an extensional stress regime involve bookshelf faulting (e.g., Mandl, 1987; Tapponnier and Courtillot, 1990; Green et al., 2014) and dog-bone seismicity (e.g., Toda et al., 2002). Bookshelf faulting contributes to the accommodation of oblique extension stress. Strike-slip earthquakes with a dog-bone-shaped distribution are induced by vertical tensile opening for strain accommodations at tips of opening cracks. However, the observed rift-parallel displacements resemble the block-like uniform movement of the graben floor and could not be explained by either bookshelf faulting or dog-bone seismicity, even if these mechanisms worked by aseismic processes.

5 Conclusions

PALSAR pixel offset and MAI data revealed as much as ~1 m of rift-parallel block-like motion for the graben floor associated with the 2005-2010 Afar rifting episode. Our observations showed rift-parallel (northwestward) horizontal motion in the northern half of the graben floor but not in the southern half. The inferred temporal evolution of rift-parallel motion in the graben floor was correlated with the evolution of the graben formation associated with dike intrusions. The rift-parallel movements on the graben floor could be reproduced by aseismic strike-slip on the graben-bounding faults since few strike-slip earthquakes were identified during 2005-2010. Based on the tectonic setting of the Afar region, we propose that strain accommodation of oblique plate spreading may be one of the possible explanations for our observations as well as for previous

observation for the Bárðarbunga dike intrusion episode, although we cannot yet provide plausible evidence to interpret the rift-parallel motion associated with the dike intrusion. We speculate that the oblique opening caused by the rotation of the Danakil block induced localized rift-parallel movements associated with the dike intrusion, although there have been few direct observations of long-term movements around the Manda Hararo-Dabbahu magmatic segment.

Acknowledgments

We appreciate two anonymous reviewers for their constructive comments to improve our manuscript. All ALOS/PALSAR level 1.0 data in this study are provided from PALSAR Interferometry Consortium to Study our Evolving Land Surface (PIXEL) group under a cooperative research contract with Earthquake Research Institute, University of Tokyo. The ownership of ALOS/PALSAR data belongs to Japan Aerospace Exploration Agency (JAXA) and Ministry of Economy, Trade and Industry (METI).

Author contribution

YH performed SAR image processing, constructed fault model and computed stress change. YH and MF managed this study, read and approved the final manuscript.

Declaration of interest

The authors declare that they have no known competing financial interests or personal relationships that could have appeared to influence the work reported in this paper.

Data availability

ALOS/PALSAR level 1.0 data are freely available through a website of ASF Data Search, supported by Alaska Satellite Facility, University of Alaska (https://search.asf.alaska.edu/).

References

Ágústsdóttir, T., Woods, J., Greenfield, T., Green, R.G., White, R.S., Winder, T., Brandsdóttir, B., Steinthórsson, S., Soosalu, H., 2016. Strike-slip Faulting During the 2014 Bárðarbunga-Holuhraun Dike Intrusion, Central Iceland. Geophys. Res. Lett. 43, 1–9.

Albers, M., Christensen, U.R., 2001. Channeling of plume flow beneath mid-ocean ridges. Earth Planet. Sci. Lett. 187, 207–220. https://doi.org/10.1016/S0012-821X(01)00276-X

Bastow, I.D., Nyblade, A.A., Stuart, G.W., Rooney, T.O., Benoit, M.H., 2008. Upper mantle seismic structure beneath the Ethiopian hot spot: Rifting at the edge of the African low-velocity anomaly. Geochemistry, Geophys. Geosystems 9.

Bechor, N.B.D., Zebker, H.A., 2006. Measuring two-dimensional movements using a single InSAR pair. Geophys. Res. Lett. 33, L16311. https://doi.org/10.1029/2006GL026883

Belachew, M., Ebinger, C., Coté, D., 2013. Source mechanisms of dike-induced earthquakes in the dabbahu-Manda Hararo rift segment in Afar, Ethiopia: Implications for faulting above dikes. Geophys. J. Int. 192, 907–917.

Calais, E., D'Oreye, N., Albaric, J., Deschamps, A., Delvaux, D., Déverchère, J., Ebinger, C., Ferdinand, R.W., Kervyn, F., Macheyeki, A.S., Oyen, A., Perrot, J., Saria, E., Smets, B., Stamps, D.S., Wauthier, C., 2008. Strain accommodation by slow slip and dyking in a youthful continental rift, East Africa. Nature 456, 783–788.

Casu, F., Manconi, A., 2016. Four-dimensional surface evolution of active rifting from spaceborne SAR data. Geosphere 12, 697–705.

Collet, B., Taud, H., Parrot, J.F., Bonavia, F., Chorowicz, J., 2000. A new kinematic approach for the Danakil block using a Digital Elevation Model representation. Tectonophysics 316, 343–357.

Corti, G., 2009. Continental rift evolution: From rift initiation to incipient break-up in the Main Ethiopian Rift, East Africa. Earth-Science Rev. 96, 1–53.

Dieterich, J.H., 1979. Modeling of rock friction: 1. Experimental results and constituve equations. J. Geophys. Res. 84, 2161–2168.

Ebinger, C., Ayele, A., Keir, D., Rowland, J., Yirgu, G., Wright, T., Belachew, M., Hamling, I., 2010. Length and timescales of rift faulting and magma intrusion: the Afar Rifting Cycle from 2005 to present. Annu. Rev. Earth Planet. Sci. 38, 439–466.

Farr, T.G., Rosen, P., Caro, E., Crippen, R., 2007. The shuttle radar topography mission. Rev. Geophys. 45, 1–33.

Furuya, M., Yasuda, T., 2011. The 2008 Yutian normal faulting earthquake (Mw 7.1), NW Tibet: Non-planar fault modeling and implications for the Karakax Fault. Tectonophysics 511, 125–133.

Grandin, R., Socquet, a., Doin, M.P., Jacques, E., De Chabalier, J.B., King, G.C.P., 2010a. Transient rift opening in response to multiple dike injections in the Manda Hararo rift (Afar, Ethiopia) imaged by time-dependent elastic inversion of interferometric synthetic aperture radar data. J. Geophys. Res. Solid Earth 115.

Grandin, R., Socquet, A., Binet, R., Klinger, Y., Jacques, E., De Chabalier, J.B., King, G.C.P., Lasserre, C., Tait, S., Tapponnier, P., Delorme, A., Pinzuti, P., 2009. September 2005

Manda hararo-dabbahu rifting event, Afar (Ethiopia): Constraints provided by geodetic data. J. Geophys. Res. 114, B08404.

Grandin, R., Socquet, A., Jacques, E., Mazzoni, N., de Chabalier, J.-B., King, G.C.P., 2010b. Sequence of rifting in Afar, Manda-Hararo rift, Ethiopia, 2005–2009: Time-space evolution and interactions between dikes from interferometric synthetic aperture radar and static stress change modeling. J. Geophys. Res. 115, B10413.

Green, R.G., White, R.S., Greenfield, T., 2014. Motion in the north Iceland volcanic rift zone accommodated by bookshelf faulting. Nat. Geosci. 7, 29–33.

Hamling, I.J., Ayele, A., Bennati, L., Calais, E., Ebinger, C.J., Keir, D., Lewi, E., Wright, T.J., Yirgu, G., 2009. Geodetic observations of the ongoing Dabbahu rifting episode: new dyke intrusions in 2006 and 2007. Geophys. J. Int. 178, 989–1003.

Hamling, I.J., Wright, T.J., Calais, E., Bennati, L., Lewi, E., 2010. Stress transfer between thirteen successive dyke intrusions in Ethiopia. Nat. Geosci. 3, 806–806.

Hamling, I.J., Wright, T.J., Calais, E., Lewi, E., Fukahata, Y., 2014. InSAR observations of post-rifting deformation around the Dabbahu rift segment, Afar, Ethiopia. Geophys. J. Int. 197, 33–49.

Hammond, J.O.S., Kendall, J.-M., Stuart, G.W., Keir, D., Ebinger, C., Ayele, A., Belachew, M., 2011. The nature of the crust beneath the Afar triple junction: Evidence from receiver functions. Geochemistry, Geophys. Geosystems 12,

Himematsu, Y., Furuya, M., 2015. Aseismic strike–slip associated with the 2007 dike intrusion episode in Tanzania. Tectonophysics 656, 52–60.

382 Himematsu, Y., Sigmundsson, F., Furuya, M., 2019. Icecap and Subglacial Crustal Deformation
383 Inferred From SAR Pixel Tracking: The 2014 Dike Intrusion Episode in the Bárðarbunga
384 Volcanic System, Iceland. J. Geophys. Res. Solid Earth 1–16.
385 Jónsson, S., Zebker, H., Segall, P., Amelung, F., 2002. Fault Slip Distribution of the 1999
386 Mw7.1 Hector Mine, California, Earthquake, Estimated from Satellite Radar and GPS
387 Measurements. Bull. Seismol. Soc. Am. 92, 1377–1389.
388 King, G.C.P., Stein, S., Lin, J., 1994. Static Stress Changes and the Triggering of Earthquakes.
389 Bull. Seismol. Soc. Am. 84, 935–953.
390 Kobayashi, T., Takada, Y., Furuya, M., Murakami, M., 2009. Locations and types of ruptures
391 involved in the 2008 Sichuan earthquake inferred from SAR image matching. Geophys.
392 Res. Lett. 36, 1–5.
393 Koptev, A., Calais, E., Burov, E., Leroy, S., Gerya, T., 2015. Dual continental rift systems
394 generated by plume–lithosphere interaction. Nat. Geosci. 8, 1–5.
395 Kreemer, C., Holt, W.E., Haines, a. J., 2003. An integrated global model of present-day plate
396 motions and plate boundary deformation. Geophys. J. Int. 154, 8–34.
397 Lohman, R.B., McGuire, J.J., 2007. Earthquake swarms driven by aseismic creep in the Salton
398 Trough, California. J. Geophys. Res. 112, B04405. https://doi.org/10.1029/2006JB004596
399 Mandl, G., 1987. Tectonic deformation by rotating parallel faults: the “bookshelf” mechanism.
400 Tectonophysics 141, 277–316.
401 McClusky, S., Reilinger, R., Ogubazghi, G., Amleson, A., Healeb, B., Vernant, P., Sholan, J.,
402 Fisseha, S., Asfaw, L., Bendick, R., Kogan, L., 2010. Kinematics of the southern Red Sea-
403 Afar Triple Junction and implications for plate dynamics. Geophys. Res. Lett. 37.

McKenzie, D., Davies, D., Molnar, P., 1970. Plate tectonics of the Red Sea and East Africa. Nature 226, 243–248.

Meade, B.J., 2007. Algorithms for the calculation of exact displacements, strains, and stresses for triangular dislocation elements in a uniform elastic half space. Comput. Geosci. 33, 1064–1075.

Pagli, C., Wang, H., Wright, T.J., Calais, E., Lewi, E., 2014. Current plate boundary deformation of the Afar rift from a 3D velocity field inversion of InSAR and GPS. J. Geophys. Res. Solid Earth.

Ruch, J., Wang, T., Xu, W., Hensch, M., Jónsson, S., 2016. Oblique rift opening revealed by reoccurring magma injection in central Iceland. Nat. Commun. 7, 12352.

Ruina, A., 1983. Slip instability and state variable friction laws. J. Geophys. Res. 88, 10359.

Saria, E., Calais, E., Stamps, D.S., Delvaux, D., Hartnady, C.J.H., 2014. Present-day kinematics of the East African Rift. J. Geophys. Res. Solid Earth 3584–3600.

Scholz, C.H., Contreras, J.C., 1998. Mechanics of continental rift architecture. Geology 26, 967–970.

Simons, M., Fialko, Y., Rivera, L., 2002. Coseismic deformation from the 1999 Mw 7.1 Hector Mine, California, earthquake as inferred from InSAR and GPS observations. Bull. Seismol. Soc. Am. 92, 1390–1402.

Sleep, N.H., 1997. Lateral flow and ponding of starting plume material. J. Geophys. Res. Earth 102, 10001–10012.

Stamps, D.S., Calais, E., Saria, E., Hartnady, C., Nocquet, J.-M., Ebinger, C.J., Fernandes, R.M., 2008. A kinematic model for the East African Rift. Geophys. Res. Lett. 35, L05304.

Strozzi, T., Luckman, A., Murray, T., Wegmüller, U., Werner, C.L., 2002. Glacier motion estimation using SAR offset-tracking procedures. IEEE Trans. Geosci. Remote Sens. 40, 2384–2391.

Takada, Y., Furuya, M., 2010. Aseismic slip during the 1996 earthquake swarm in and around the Onikobe geothermal area, NE Japan. Earth Planet. Sci. Lett. 290, 302–310.

Tapponnier, P., Courtillot, V., 1990. Bookshelf faulting and horizontal block ratations between overlapping rifts in southern Afar. Geophys. Res. Lett. 17, 1–4.

Tobita, M., Murakami, M., Nakagawa, H., Yarai, H., Fujiwara, S., Rosen, P.A., 2001. 3-D surface deformation of the 2000 Usu Eruption measured by matching of SAR images. Geophys. Res. Lett. 28, 4291–4294.

Toda, S., Stein, R.S., Sagiya, T., 2002. Evidence from the AD 2000 Izu islands earthquake swarm that stressing rate governs seismicity. Nature 419, 58–61.

Vidale, J.E., Shearer, P.M., 2006. A survey of 71 earthquake bursts across southern California: Exploring the role of pore fluid pressure fluctuations and aseismic slip as drivers. J. Geophys. Res. Solid Earth 111, 1–12.

Wegmüller, U., Werner, C.L., 1997. Gamma SAR processor and interferometry software. Proc. 3rd ERS Symp. Eur. Sp. Agency Spec. Publ. 1687–1692.

Wicks, C., Thelen, W., Weaver, C., Gomberg, J., Rohay, A., Bodin, P., 2011. InSAR observations of aseismic slip associated with an earthquake swarm in the Columbia River flood basalts. J. Geophys. Res. 116, B12304.

Wright, T.J., Ebinger, C., Biggs, J., Ayele, A., Yirgu, G., Keir, D., Stork, A., 2006. Magma-maintained rift segmentation at continental rupture in the 2005 Afar dyking episode. Nature 442, 291–294.

Wright, T.J., Lu, Z., Wicks, C., 2003. Source model for the Mw 6.7, 23 October 2002, Nenana Mountain Earthquake (Alaska) from InSAR. Geophys. Res. Lett. 30, 30–33.

Wright, T.J., Sigmundsson, F., Pagli, C., Belachew, M., Hamling, I.J., Brandsdóttir, B., Keir, D., Pedersen, R., Ayele, A., Ebinger, C., Einarsson, P., Lewi, E., Calais, E., 2012. Geophysical constraints on the dynamics of spreading centres from rifting episodes on land. Nat. Geosci. 5, 242–250.

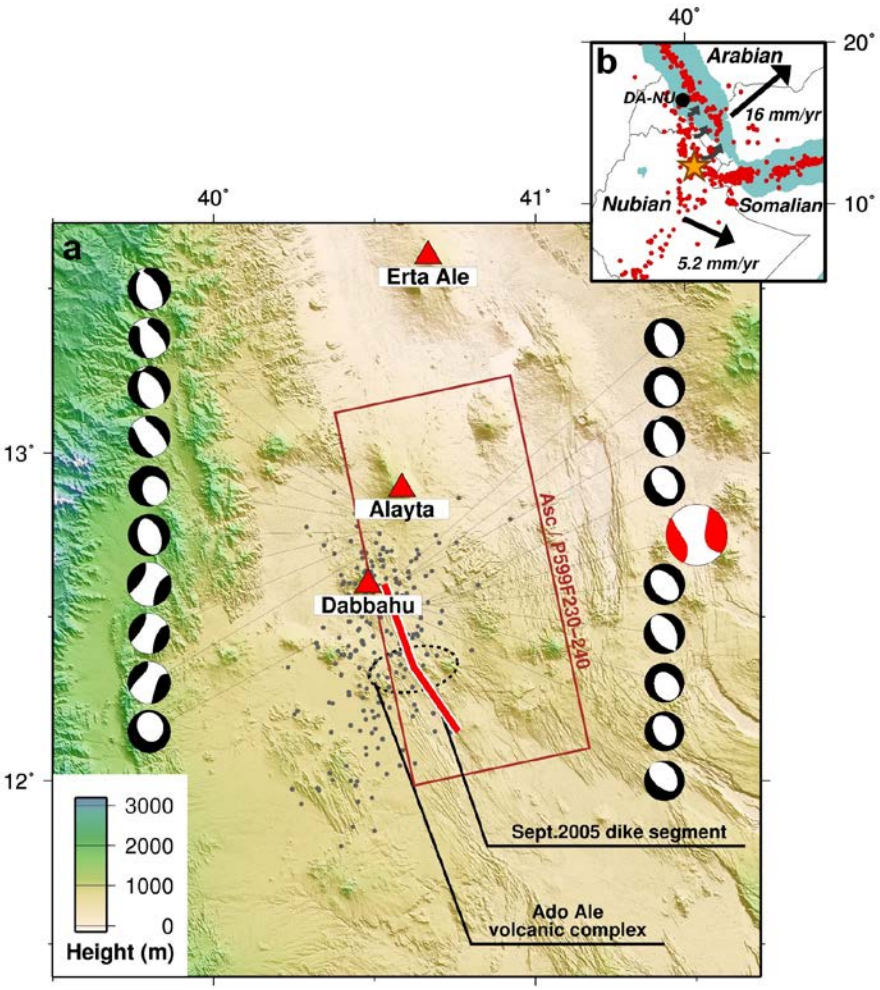

Fig. 1. Summary map of the study area. (a) Gray dots show epicentral locations of earthquake swarm during 2005-2010 from USGS catalogue. Black beach-balls are focal mechanisms of M>4.9 earthquakes during the period. Large red beach-ball is that of the greatest earthquake (M 5.5, 24 Sep. 2005). Red triangles indicate locations of active volcanoes around the Manda Harraro-Dabbahu segment. Red rectangular traces a footprint of the L-band PALSAR radar images. (b) Location map around Afar depression. Black arrows indicate relative plate velocities in a Nubian-fixed reference frame. Gray curved vectors and ~~dashed circle~~ black dot indicate the schematic relative motion and the rotation pole of the Danakil block reference to Nubian plate (McClusky et

al., 2010). Red dots locate earthquake epicenters during 1960-2010. Star marks the location of the study area.

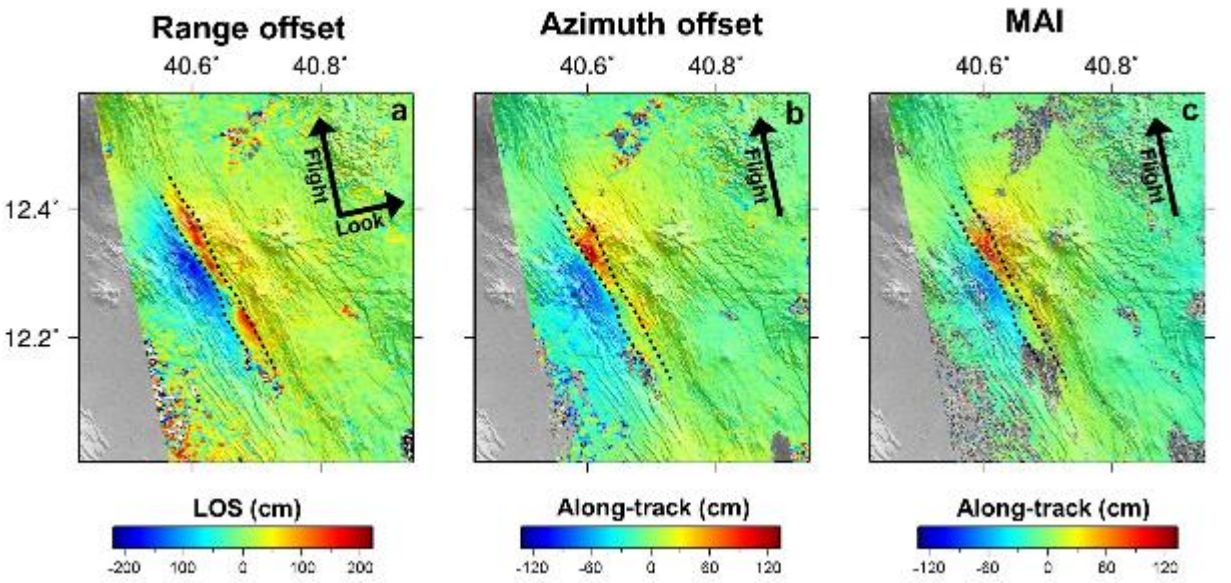

Fig. 2. Cumulative displacements from 12 June 2007 and 5 August 2010 from PALSAR data. Range offset (a) shows the displacement along the line-of-sight. Both azimuth offset (b) and MAI (c) are sensitive to the horizontal displacement along the satellite flight direction. Positive values (red color) indicate displacements away from the satellite along the line-of-sight (LOS) direction in the range offset and horizontal displacements to the satellite flight direction in the azimuth offset and MAI, respectively. Top-right arrows show the satellite flight direction (Flight, N349E°) and line-of-sight (Look). Black dot lines are top locations of two graben-bounding faults.

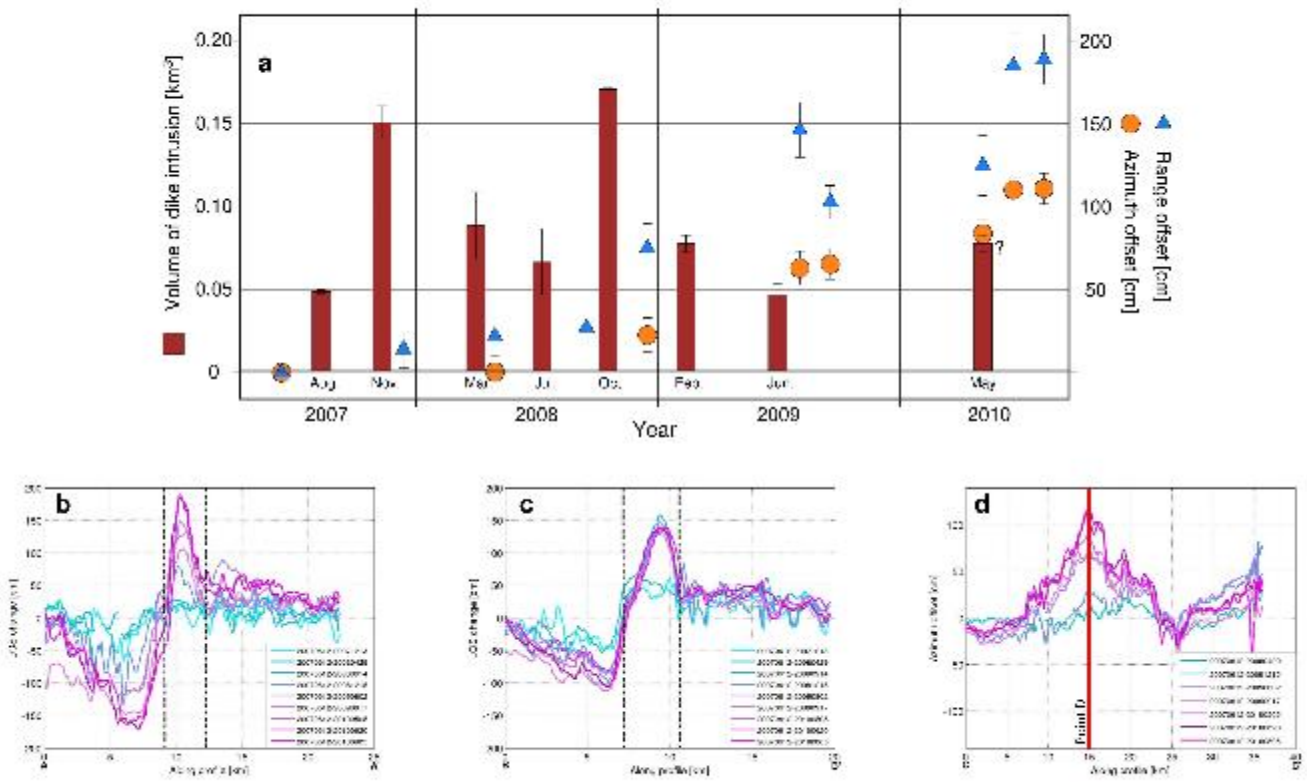

Fig. 3. (a) Volume of dike intrusion and temporal evolution of range offset and azimuth offset on the northern part of the graben floor. Left-vertical axis shows volume of magma intrusion (Red bars) whose data are shown in Hamling et al. (2009) and Wright et al. (2012). Right-vertical axis shows range offset (Blue triangle) and azimuth offset (Orange circles) on the northern part of the graben floor (Point D). Vertical error bars represent the root-mean-squares at the non-displacement field in each of the results. (b-d) Temporal evolution of the range and azimuth offset along each cross-section in Fig. S1 in the Supplementary Material. Black dashed lines are the location of the graben-bounding fault.

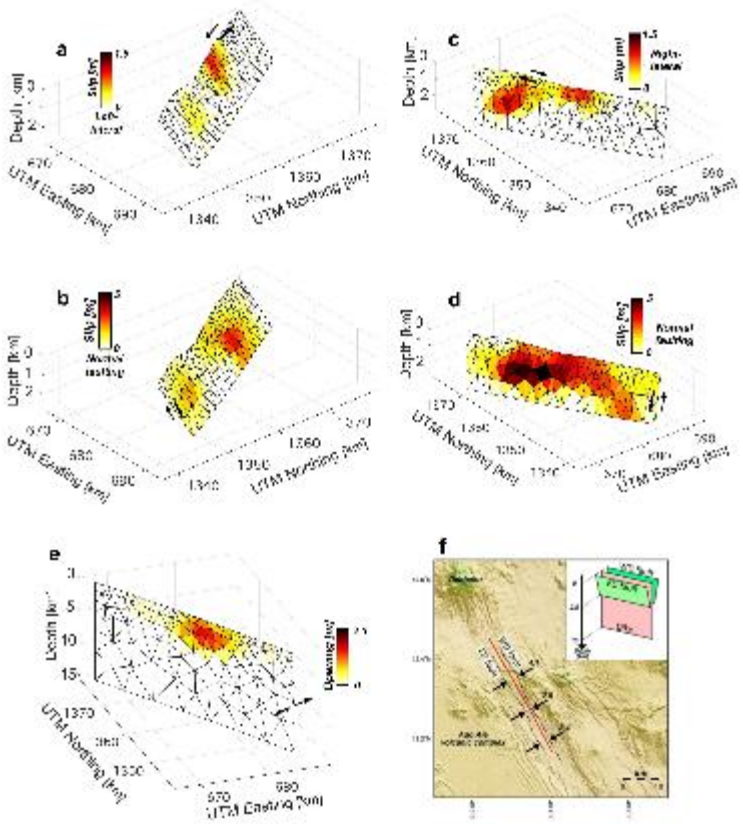

Fig. 4. Best-fit slip-distributions. Right-lateral strike-slip (a) and normal faulting (b) on the east-dipping fault. Left-lateral strike-slip (c) and normal faulting (d) on the west-dipping fault. (e) Dike opening distribution. (f) Overview and geometry of the fault model. Black and red lines indicate top locations of the two faults and the dike segments, respectively. Numbers with black arrows are graben widths at each point. Inset shows schematic image of fault model geometry.

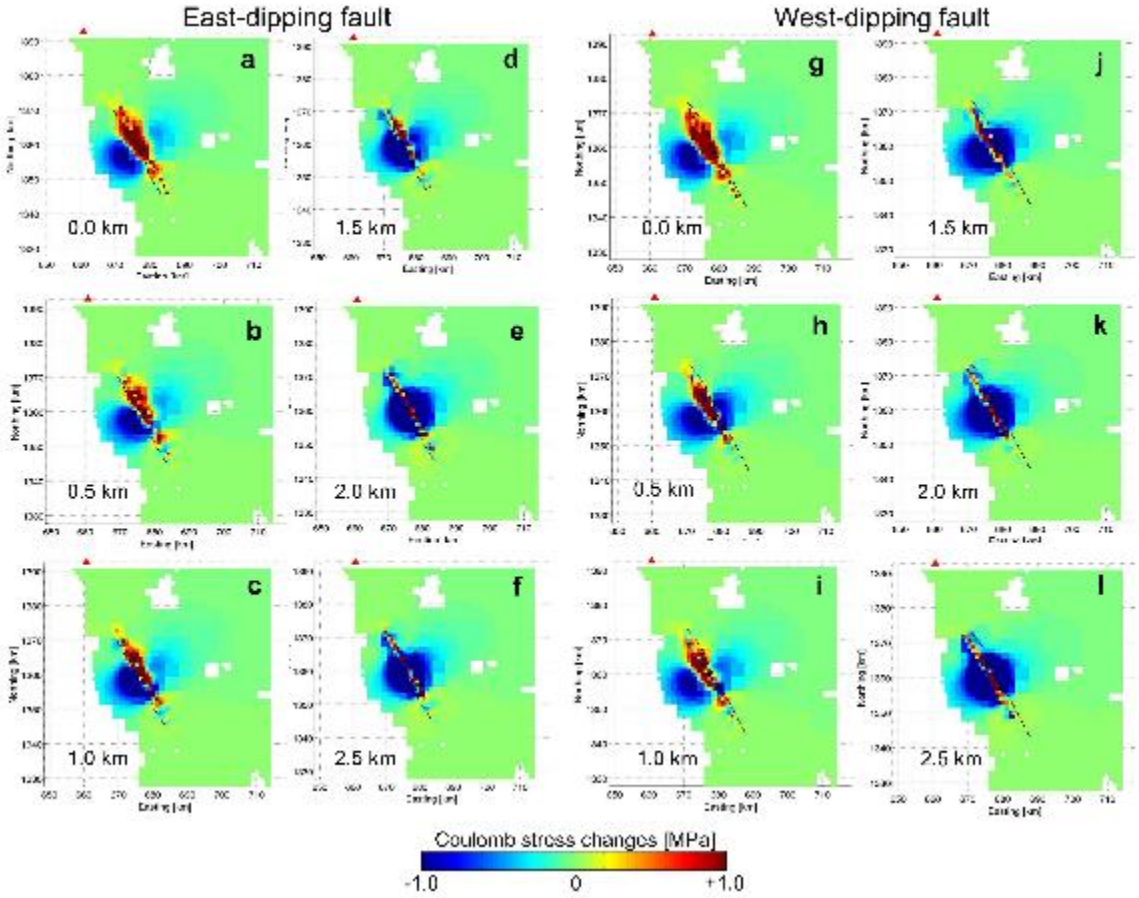

Fig. 5. Coulomb stress changes due to dike opening. Horizontal slices of stress changes associated with dike opening inferred from our model on east-dipping fault (a-f) and west-dipping fault (g-l). Depths of slice are shown at bottom-left corner of each panel. Positive stress changes indicate promoting fault slip on receiver fault. Black dashed lines show top locations of each receiver fault. Red triangles located at the Dabbahu volcano.